

ARTICLE

Received 12 Oct 2012 | Accepted 13 Mar 2013 | Published 30 Apr 2013

DOI: 10.1038/ncomms2734

All-optical polariton transistor

D. Ballarini^{1,2}, M. De Giorgi^{1,2}, E. Cancellieri^{3,4}, R. Houdré⁵, E. Giacobino⁴, R. Cingolani¹,
A. Bramati⁴, G. Gigli^{1,2,6} & D. Sanvitto^{1,2}

Although optical technology provides the best solution for the transmission of information, all-optical devices must satisfy several qualitative criteria to be used as logic elements. In particular, cascability is difficult to obtain in optical systems, and it is assured only if the output of one stage is in the correct form to drive the input of the next stage. Exciton-polaritons, which are composite particles resulting from the strong coupling between excitons and photons, have recently demonstrated huge non-linearities and unique propagation properties. Here we show that polariton fluids moving in the plane of the microcavity can operate as input and output of an all-optical transistor, obtaining up to 19 times amplification and demonstrating the cascability of the system. Moreover, the operation as an AND/OR gate is shown, validating the connectivity of multiple transistors in the microcavity plane and opening the way to the implementation of polariton integrated circuits.

¹Istituto Italiano di Tecnologia, IIT-Lecce, Via Barsanti, 73010 Lecce, Italy. ²NNL, Istituto Nanoscienze—CNR, Via Arnesano, 73100 Lecce, Italy. ³Fisica Teorica de la Materia Condensada, Universidad Autonoma de Madrid, 28049 Madrid, Spain. ⁴Laboratoire Kastler Brossel, Université Pierre et Marie Curie-Paris 6, École Normale Supérieure et CNRS, UPMC Case 74, 4 place Jussieu, 75005 Paris, France. ⁵Institut de Physique de la Matière Condensée, Faculté des Sciences de Base, Bâtiment de Physique, Station 3, EPFL, CH-1015 Lausanne, Switzerland. ⁶Innovation Engineering Department, University of Salento, Via Arnesano, 73100 Lecce, Italy. Correspondence and requests for materials should be addressed to D.B. (email:dario.ballarini@iit.it).

Light beams can carry information over long distances, and have proved to be better than electronic wires for low-loss transmissions at high data rate. Moreover, optical connections can, in principle, operate faster and with lower energy consumption than electronic ones even at very short distances, down to chip interconnects^{1,2} with the not negligible advantage of having very low dissipations and virtually no heating. However, the implementation of high-speed, low-energy, optical logics in all-optical integrated circuits represents a big challenge for future information processing³. Several systems have been proposed and studied to develop all-optical switches, including Mach–Zehnder interferometers in semiconductor materials⁴, spin polarization in multiple quantum wells⁵, waveguide-coupled ring resonator in silicon⁶, photonic crystal nanocavities⁷ and polarization bistability in vertical cavity emitting structures⁸. However, to be used as a logic element in an integrated circuit, a switch must satisfy some critical conditions such as cascability (the output and input should be compatible to allow for connections in series of several devices) and the possibility to feed with one output several inputs (fan-out or gain) and vice versa (fan-in)^{9,10}.

In this context, microcavity polaritons, the quantum superposition of electron-hole pairs (excitons) and light (photons), are a peculiar and interesting kind of semiconductor quasi-particles. In fact, polaritons inherit from their photonic part the very light mass (10^{-4} times that of an electron) and high speed (1% of the speed of light), which yields fast switching times¹¹, while their electronic component provides strong nonlinear effects at power thresholds orders of magnitude lower than in standard dielectrical optical crystals^{12–25}. Recently, the observation of a non-equilibrium condensed phase^{26,27} of polaritons paved the way to the study of new quantum phenomena, which could lead to virtually loss-free operations and communication^{28–32} up to room temperature³³. Their potential use for logical operations has also been explored in recent proposals^{34,35}, where the information is carried by polariton quasi-particles propagating inside the plane of the microcavity along integrated circuits based on ‘polariton neurons’³⁶. On the other hand, lateral confinement of flowing polaritons has been realized by modelling the photonic potential of the cavity through precise etching of the structure, obtaining propagation distances of more than 200 μm (ref. 37).

In this Article, we experimentally demonstrate the working principle of a polariton transistor in semiconductor planar microcavities based on the nonlinear interactions between two polariton fluids. The power threshold for nonlinear absorption of a polariton state (Address) is tuned by the injection of a small polariton population (Control), showing a ratio between Address and Control densities of more than one order of magnitude (12 dB). We show that the output of one transistor is a polariton fluid propagating in the plane of the microcavity, which is in the correct form to work as a Control signal for the switching on of a second, spatially separated, transistor, therefore demonstrating the cascability of the system. Moreover, the functionality of the polariton transistor is further extended through the implementation of the AND and OR gates, where two propagating polariton fluids are used as inputs for the gate, allowing the proper control of the output level.

Results

Experimental configuration. Our experiments have been performed in transmission configuration and at a temperature of 10 K. A sketch of the experimental configuration is reported in Fig. 1a: a single mode, continuous wave, laser beam impinges on a GaAs/AlAs microcavity, composed by front and back distributed Bragg reflectors (DBRs) with 21 and 24 pairs, respectively, and

three $\text{In}_{0.04}\text{Ga}_{0.96}\text{As}$ quantum wells embedded in the microcavity plane. The laser beam is partially reflected from the front DBR, which only allows the penetration of those frequencies that match with the polariton dispersion (shown in Fig. 1b). The angle of incidence of the laser beam with respect to the direction perpendicular to the sample corresponds to the in-plane momentum of the resonantly created polaritons, which propagate with a finite velocity in the microcavity plane (downward direction in the sketch of Fig. 1a). Owing to the finite polariton lifetime in the microcavity (around 10 ps), this process can be observed through the photon emission from the back DBR: the polariton density in each state is proportional to the emission intensity, which is recorded both in real and momentum space by a CCD coupled to a spectrograph and directly measured by a power meter. In the experiments described in the following, we used linearly polarized beams to avoid the effect of the spin on the dynamics of the system. Although the additional degree of freedom constituted by the polariton spin can be advantageous in future devices³⁸, we will focus here on the demonstration of the basic transistor operation and its connectivity.

Blueshift mechanism. An important mechanism which has a key role in this resonant scheme is the renormalization of the polariton energies with increasing polariton densities. Owing to the polariton–polariton interactions, originated from their excitonic components, the polariton resonance is indeed shifted towards higher energies when the polariton density increases. In the case of optical excitation, if the pumping laser is slightly detuned above the polariton resonance, two different regimes can be distinguished. For low enough polariton densities, the laser remains out of resonance (the ‘off’ regime), while for densities above a certain threshold the polariton energy jumps into resonance with the pump energy, resulting in a dramatic increase of the population of the pumped state. This behaviour is shown in Fig. 1c for the polariton state called Address in this work and described in the following subsection. On the contrary, if the pumping laser is set at resonance with the polariton energy, the polariton density increases linearly until absorption is saturated by the pump-induced blueshift. This is the case for the Control state described below.

Address and Control state. In the first part of the experiment we create both Address and Control states by external optical injection, measuring the polariton density in the Control needed to switch on the Address. The laser beam has been divided in two paths, which impinge with different angles on the microcavity plane in order to resonantly excite two states of the lower polariton branch, Control and Address, which share the same energy, $E_C = E_A$, but have different finite momenta in the microcavity plane, \mathbf{K}_C and \mathbf{K}_A respectively. We will see in the second part of the experiment that the control operation can be performed by internal signals, without the need for external laser excitation of the Control state.

In the upper panel of Fig. 1b, the two-dimensional momentum space (K_x, K_y) image of the emission shows the Control ($K_x = K_C, K_y = 0$) and Address ($K_x = K_A, K_y = 0$) states, which are saturated in order to appreciate the weak emission from the microcavity ring due to laser elastic scattering. In the lower panel of Fig. 1b, the polariton dispersion along $K_y = 0$, is shown under non-resonant, low power, excitation. The Control and Address momenta, $K_C = -1 \mu\text{m}^{-1}$ and $K_A = 0.5 \mu\text{m}^{-1}$, are indicated by solid vertical lines, while the pumping energy $E = 1.481 \text{ eV}$ is indicated by a dashed horizontal line. We choose this configuration in order to have the detuning $\Delta E_{A,C} = E_{\text{laser}} - E_{A,C}$ between the excitation energy E_{laser} and the polariton resonance $E_{A,C}$ for the Address and

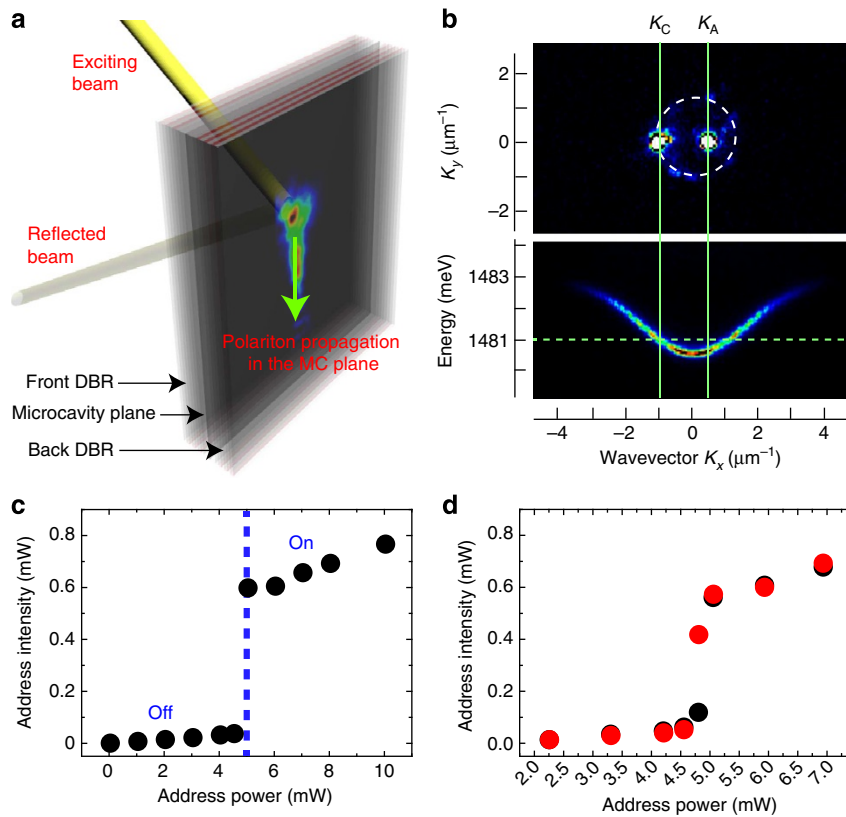


Figure 1 | Experimental configuration and switch on of the Address. (a) Sketch of the experimental configuration: the exciting laser beam is directed with an angle on the microcavity sample and partially reflected from the front DBR. Polaritons are created within the microcavity plane and propagate with a finite velocity. The one-to-one coupling with the external photons allows the observation of the polariton propagation through the emitted intensity from the back side of the sample. (b) In the upper panel, the two-dimensional momentum space image of the emission under high excitation power shows the polariton states created by two laser beams impinging at different angles (K_C and K_A) and same energy. The lower panel shows the polariton dispersion along the direction corresponding to $K_y = 0$ of the upper panel. The vertical lines indicate the value of $K_A = 0.5 \mu\text{m}^{-1}$ and $K_C = -1 \mu\text{m}^{-1}$ and the horizontal line indicates the pumping energy $E = 1.481$ eV. (c) The emission intensities of the address state are plotted for increasing powers of the exciting beam. The Address powers are measured from the laser before arriving on the microcavity sample. (d) Measurements of the hysteresis cycle around the threshold of panel (c). Black and red dots correspond to points of the onwads and backwards power changes, respectively, showing the absence of the hysteresis power-cycle.

Control state tuned to $\Delta E_A = 0.4$ meV and $\Delta E_C \approx 0$, respectively.

Owing to the slight detuning of the Address state with respect to the laser beam, the polariton population in this state follows the nonlinear behaviour shown in Fig. 1c, where the emission intensity I_A of the Address state is plotted as a function of the power of the pumping laser. Note that, although the powers of the lasers beams are measured before arriving on the microcavity sample, the amount of light intensity that has penetrated the front microcavity mirror are obtained from the intensities of the Address and Control states, I_A and I_C , measured by the photon emission from the back DBR and which correspond to the polariton population in each state. As shown in Fig. 1c, the Address population increases abruptly at the power threshold $P_{\text{th}}^A = 5$ mW. Increasing further the exciting power, saturation will eventually occur because of the blueshift of the polariton branch with respect to the exciting energy. It is important to note here that the detuning ΔE_A has been set in a way that any hysteresis cycle (bistable regime) is avoided¹⁸. Indeed, decreasing the detuning between the exciting energy and the polariton resonance, the width of the hysteresis loop, typical of the optical bistability regime, shrinks towards the presence of only one threshold (optical discriminator regime)³⁹. In order to verify that we actually are in this regime, we repeated the measurements of the address intensities under increasing and decreasing excitation powers around the threshold, as shown in Fig. 1d.

The black and red dots correspond to points of the onwads and backwards power changes, respectively. As can be seen, the curve is overlapping, showing the absence of the hysteresis power-cycle. This is an important experimental condition to set, in order to obtain a proper control of the switching property.

Conversely, as the Control state is in resonance with the exciting beam, the injection of polaritons occurs with a linear increase of the population even at very low powers, with power-independent insertion losses of 10 dB.

The principle of the transistor is to use only a small polariton density in the Control state to switch on a much higher polariton density in the Address state. This is indeed possible due to the combination of repulsive interactions between polaritons in different states and the peculiar dispersion given by the light field⁴⁰. Once the Address signal is activated by the external Control, it can be used, in turn, as an internal Control for the next-in-series transistor, in a cascade configuration interconnected through the polariton propagation in the plane of the microcavity, as it will be shown later in this work.

Transistor operation. In Fig. 2a, the characteristic curves of the Address intensity I_A are shown for different values of I_C . The threshold power P_{th}^A lowers when increasing the control density, passing from $P_{\text{th}}^A = 5$ mW in the case of no control beam to

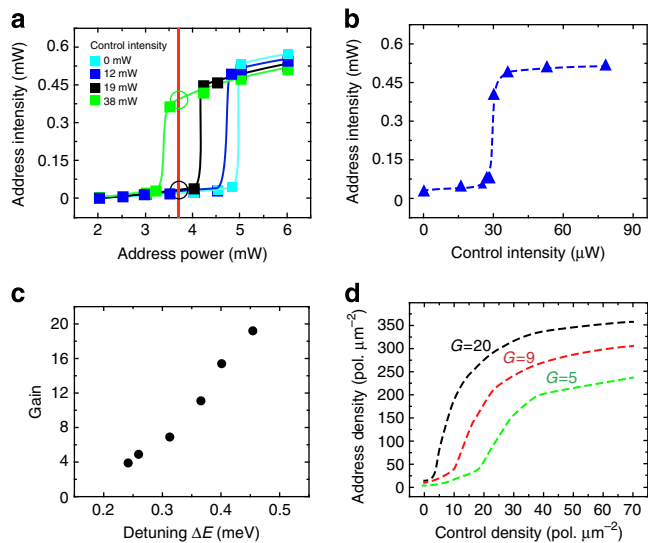


Figure 2 | Transistor operation. (a) Address intensity plotted as a function of the Address power for different intensities of the Control: green line ($I_C = 38 \mu\text{W}$), black line ($I_C = 19 \mu\text{W}$), blue line ($I_C = 12 \mu\text{W}$) and without control (light blue line). The red line indicates the power of the Address for which a small change in the Control density brings the Address state from off (black circle) to on (green circle). (b) Address intensities against Control intensities taken for an address power of $P^A = 3.7 \text{ mW}$, corresponding to the position of the red line in (a). The gain is measured as the ratio between the emission intensities of Address and Control at threshold, $G = I_A/I_C$. (c) The amplification (I_A/I_C) at threshold is plotted as a function of the energy detuning ΔE_A between the exciting laser and the polariton branch. The gain increases for higher detuning ΔE_A , showing the possibility to modulate the amount of amplification. (d) Simulations of the Address densities as a function of the Control density and corresponding gain G for different Address powers, measured in units of the Address threshold P_{th}^A : $0.70P_{\text{th}}^A$ ($G = 5$), $0.76P_{\text{th}}^A$ ($G = 9$) and $0.83P_{\text{th}}^A$ ($G = 20$), corresponding to the green, red and black colour, respectively.

$P_{\text{th}}^A = 3.5 \text{ mW}$ in correspondence of a control intensity of $38 \mu\text{W}$. Therefore, for a fixed value of P^A , the Address can be switched on (green circle in Fig. 2a) and off (black circle in Fig. 2a) by changing the polariton density in the Control state.

This operational principle is verified in Fig. 2b, where the Address intensity (blue triangles) is plotted as a function of the Control intensity for $P^A = 3.7 \text{ mW}$, corresponding to the red line in Fig. 2a. The address is switched on (off) for Control intensities I_C above (below) the threshold of $30 \mu\text{W}$. The extinction ratio of the Address intensity below and above threshold is $r_e > 10$. The gain G is defined as the ratio between the polariton density in the Address above threshold and the polariton density in the Control state required for the switching operation, and it is directly obtained by measuring the emission intensities of Address and Control at threshold, $G = I_A/I_C$. Note that the gain is defined only by the emission intensities, which are directly related to the number of polaritons inside the cavity. Indeed, the gain requirement consists in the fact that few polaritons in the Control must be able to switch on enough polaritons in the Address so that, moving in the plane they can act as a Control for the next transistor in cascade. In this case, a gain $G = 15$ is obtained, showing that the density of the Address is more than one order of magnitude larger than the polariton density in the Control. This threshold corresponds to a density between 5 and 20 polaritons per μm^2 in the Control state, which means few attojoule per μm^2 . Even considering the relatively wide laser spot used in these

experiments to avoid any diffraction effect due to finite cavity width, the polariton population in the whole area is anyhow reaching, at most, an energy of few femtojoule, figure which could be strongly reduced by, for instance, designing *ad hoc* waveguides and mesa structures with lateral size down to few micrometres.

An interesting point is that the value of the amplification at threshold can be modulated by tuning the energy of the exciting laser, obtaining a higher gain when the detuning of the Address ΔE_A is increased, as shown in Fig. 2c. The range of energy detuning ΔE_A for which the system is still in the optical discriminator regime is wide enough to allow a modulation of the gain from 4 to 19 (note that, in order to obtain a higher gain for larger detuning, the Address power has to be increased accordingly). The polariton densities of Control and Address have been theoretically simulated and confirm the experimental observation of a strong gain at threshold, which is triggered by a polariton density lower than 10 polariton per μm^2 in the Control state. These numbers can be improved even further with microcavities of higher finesse and by reducing the Address detuning (though, in this case, with a trade-off of a smaller gain). In Fig. 2d, the simulations are run for three different powers of the Address beam ($0.70P_{\text{th}}^A$, $0.76P_{\text{th}}^A$ and $0.83P_{\text{th}}^A$, corresponding to the green, red and black colour, respectively), showing that the control threshold can be lowered by tuning, for instance, the Address power.

Propagation and cascability. We are now interested in the possibility to demonstrate full cascability by triggering the absorption of a second Address beam, spatially separated from the first, through the propagation of polaritons within the plane of the microcavity. This scheme, sketched in Fig. 3a,b, can be seen as two transistors in series in which the first input controls the second's output. In order to do so, the real and momentum space images of the emission intensities have been simultaneously recorded for the whole area comprising the two transistors. As shown in Fig. 3, the second Address beam (labelled B in Fig. 3) is focused at a distance of $40 \mu\text{m}$ from the first Address (labelled A), both A and B being below threshold (Fig. 3c,d for real and momentum space, respectively). Note that the Control beam (labelled C) is spatially overlapping only with beam A and having orthogonal momentum. In Fig. 3d, the two-dimensional image of the momentum space shows that the momenta of A, B and C in the microcavity plane point in different directions. When the density of C is increased the polariton fluid propagates from point A towards point B, bringing above threshold the second Address B, which in turn propagates in the perpendicular direction. This is shown in Fig. 3e,f, for real and momentum space, respectively, with a colour scale corresponding to 20 times higher intensity with respect to the off regime of Fig. 3c,d. When the Control density in the first transistor is lowered below threshold, both A and B switch off.

AND and OR gates. Interestingly, two or more Controls can contribute to the activation of the Address, furnishing the basis for the operation of the transistor as a logic gate. We explore here the possibility to use two propagating polariton fluids (labelled A and B in Fig. 4) to control the output of a third transistor (labelled C in Fig. 4). Both A and B are separated by a distance of about $70 \mu\text{m}$, while C is placed near the intersection point of A and B, as shown in Fig. 4, and directed horizontally rightward. The transistor C is indeed working as an AND gate if the threshold is reached when both A and B are on (right column of Fig. 4), while it is working as an OR gate if A or B only are required for the activation of C (left column of Fig. 4). In Fig. 4, the AND gate is obtained by lowering the Address power of C by 10% with respect

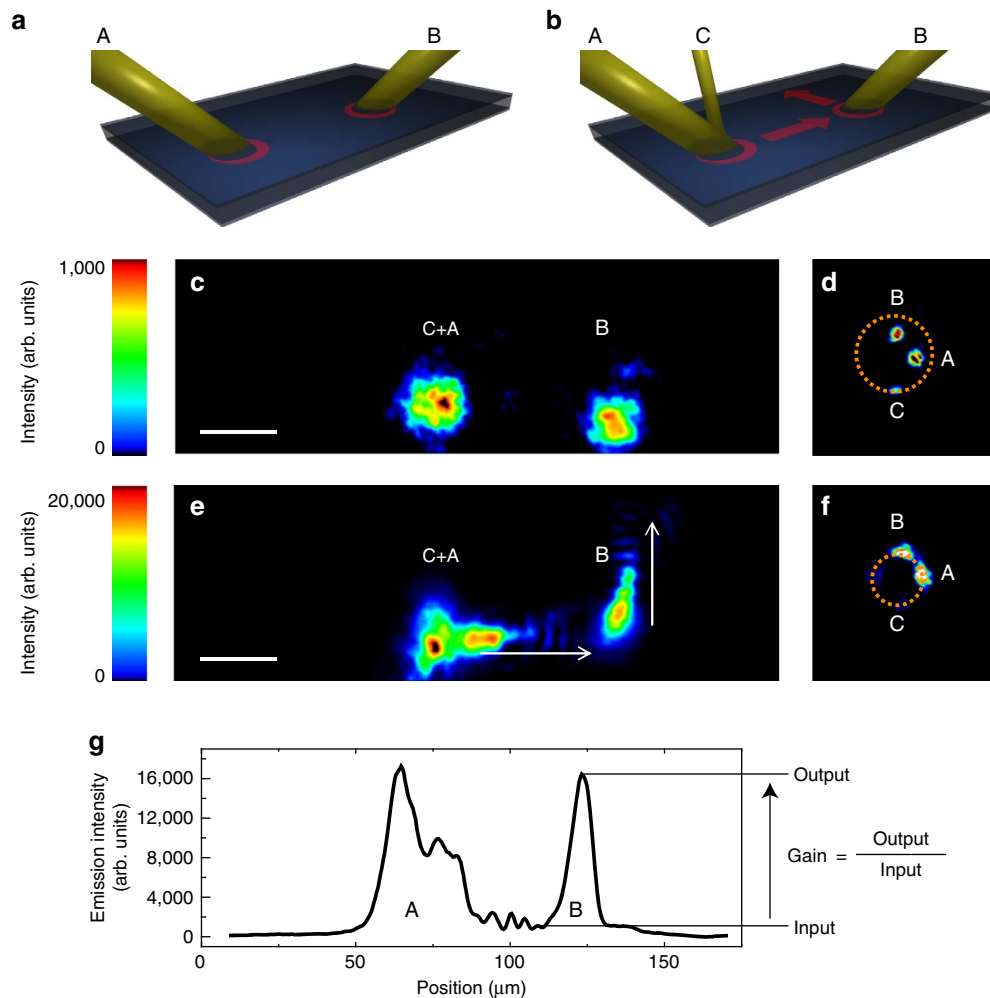


Figure 3 | Propagation and cascability. (a) Scheme of the experimental configuration with two Address beams focused in separated points of the sample with different incident angles. (b) Scheme of the polariton propagation when the Control C is focused over Address A, with the red arrows indicating the propagation direction of the respective polariton states. (c) Real space image of the emission intensities of the Address A and B, and of the Control C below threshold. Scale bar, 25 μm. (d) Far field image of the emission intensities showing the momenta of A, B and C. The circle corresponds to the position of the elastic scattering ring. (e) Real space image of the propagating states A and B, above threshold thanks to the small increase of the intensity of C (same powers as in Fig. 2). Note that the intensity in panel (c) has been multiplied 20 times in order to get the same colour scale as in panel (e). Scale bar, 25 μm. (f) In momentum space, A and B are now on resonance with the laser energy and their intensities increase abruptly, while the intensity of C is negligible. (g) Emission intensity profile along the horizontal direction and graphic representation of the gain G.

to the OR case. In this way, we are slightly reducing the gain in the AND gate. Owing to the nonlinear behaviour of the transistor, the difference is only of about 10% of the Address power and it doesn't affect significantly the output level, being the extinction ratio $r_e > 10$ even for the AND gate. The upper panel of Fig. 4 shows the off state, when both the Controls of A and B are below threshold.

Discussion

Optical amplification and switching can be obtained in strongly coupled exciton-photon systems through the peculiar non-linear properties of microcavity polaritons. The light-matter nature of these quasi-particles allows us to obtain switching times of the order of the cavity lifetime (10 ps), with the additional advantage of using ultra low-activation energies (1 fJ). The results presented in this Article show that using polariton states with finite velocities it is possible to realize an all-optical transistor, which is based on the propagation of polariton fluids in the chip plane. The on-state propagates out of the injection region towards a

second injection point, being able to activate a new polariton fluid with different velocity and direction. Even with the complication to guide polariton fluids in the planar (two-dimensional) microcavity used in this experiment, we demonstrate that one transistor is able to trigger the on state of another transistor spatially separated from the first. This operation takes place all inside the microcavity, allowing for multiple interconnections to occur in the plane of the semiconductor chip. We have shown the amplification properties of the transistor in Fig. 2, and proven the cascability of the system in the experiments of Fig. 3. Indeed, amplification and cascability are both essential requirements for the connectivity of more transistors in the same circuit. This is further proven in Fig. 4, where two outputs are used as inputs into one transistor, enabling the AND/OR logic operation as a three terminal system (two inputs and one output). Finally, looking at Fig. 2b, it can be observed that the on-state intensity of the output is almost independent from the input intensity (above threshold). This allows the connection of multiple inputs into the same gate, restoring the correct output level.

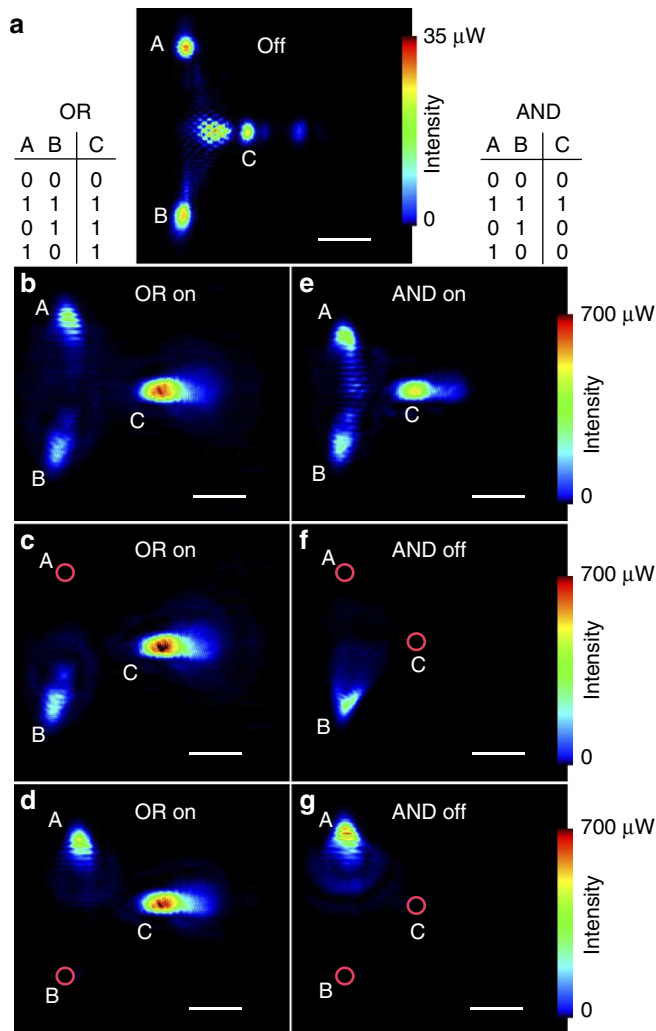


Figure 4 | AND and OR logic gates. Three transistors scheme (A, B and C, spatially separated by a distance of about $30\ \mu\text{m}$) in which C acts as AND/OR logic gate with inputs A and B. When A, B and C are below threshold as in (a), their output intensities are lower than $35\ \mu\text{W}$. The interference pattern originated by the three fluids is visible near the intersection point in this low-density regime. Owing to the increase of the intensities above threshold, the colour scales in panels (b–g) are reduced by a factor 20 as compared with panel (a). The OR gate is described in the left column with both A and B on (b), B only on (c), A only on (d). C is always activated when A or B or both are on. The AND gate is obtained by lowering 10% the Address power of C, and it is described in the right column with both A and B on (e), B only on (f), A only on (g). It is required that both A and B are on to activate C. Red circles in panels (c,d,f,g) indicate the positions of the off states. Scale bars, $20\ \mu\text{m}$. The corresponding logic tables are resumed on top of each column.

The results presented so far provide the basis for the integration of polariton systems in future realization of all-optical circuits. In this context, further investigations on the hydrodynamic properties of polaritons should be dedicated to the design of suited geometries for the division and coupling of polariton fluids in guiding structures. In particular, the propagation properties and footprint can be strongly improved using one-dimensional polariton wires etched in high-quality samples ($Q > 20,000$). Note that, in this case the finite velocity of the polariton fluids can be controlled independently of the angle of incidence of the injection laser, for example, by providing an

exciton-photon detuning with a gradient in the desired direction⁴¹ or by controlling the expansion of the polariton fluid³⁷. In addition to the classic gates, 0D pillar structures could be also used to exploit the energy quantisation and other phenomena typical of localised superfluids such as the Josephson effects or the conditional tunnelling. This device shows an interesting potential for future optical operation, which could take advantage of the ultra-fast clock cycles and ultra low-energy dissipation of all-optical polaritonic signals.

Methods

Two-component Gross-Pitaevskii equation. A standard way to model the dynamics of the system of resonantly-driven polaritons in a planar microcavity is to use a Gross-Pitaevskii equation for coupled cavity and exciton field (ψ_C and ψ_X) generalized to include the effects of the resonant pumping and decay ($\hbar = 1$):

$$i\partial_t \begin{pmatrix} \psi_X \\ \psi_C \end{pmatrix} = \begin{pmatrix} 0 \\ F \end{pmatrix} + \left[\hat{H}_0 + \begin{pmatrix} g_X |\psi_X|^2 & 0 \\ 0 & V_C \end{pmatrix} \right] \begin{pmatrix} \psi_X \\ \psi_C \end{pmatrix} \quad (1)$$

where the single particle polariton Hamiltonian H_0 reads:

$$\hat{H}_0 = \begin{pmatrix} \omega_X - ik_X & \Omega_{R/2} \\ \Omega_{R/2} & \omega_C(-i\nabla) - ik_C \end{pmatrix}$$

where $\omega_C(-i\nabla) = \omega_C(0) - \frac{\nabla^2}{m_c}$ is the cavity dispersion as a function of the in-plane wave vector and where the photon mass is $m_c = 2 \times 10^{-5} m_0$ and m_0 is the bare electron mass. For these simulations, a flat exciton dispersion relation $\omega_X(k) = \omega_X(0)$ will be assumed and the case of zero detuning at normal incidence $\omega_X(0) = \omega_C(0)$ considered. The parameters Ω_R , k_X and k_C are the Rabi frequency and the excitonic and photonic decay rates, respectively, and are taken close to experimental values: $\Omega_R = 5.0\ \text{meV}$, $k_X = 0.001\ \text{meV}$ and $k_C = 0.1\ \text{meV}$. In this model, polaritons are injected into the cavity in two states (address and control) by two coherent and monochromatic laser fields. The two laser fields share the same smoothen top-hat spatial profile with intensities F_A and F_C for the address and the control, respectively, and with full width at half maximum equal to $60\ \mu\text{m}$. The two laser fields share also the same frequency ω but have different in-plane momentum $k_A = 0.5\ \mu\text{m}^{-1}$ and $k_C = -0.7\ \mu\text{m}^{-1}$. The exciton-exciton interaction strength g_X is set to one by rescaling both the cavity and excitonic fields and the pump intensities. Our theoretical results come from the numerical solution of equation (1) over a two-dimensional grid (256×256) in a $140 \times 140\ \mu\text{m}^2$ box using a fifth-order adaptive-step Runge-Kutta algorithm. All the analysed quantities are taken when the system has reached the steady state condition after 1,000 ps. The number of polaritons in the control state at thresholds results to be 3, 5 and 7 polaritons per μm^2 for the black, red and green curve in Fig. 4d, respectively.

Evaluation of the polariton (pol) densities. For a measured address emission $I = 0.5\ \text{mW}$, we obtain a density $N = I\tau/(EA) \approx 70\ \text{pol per } \mu\text{m}^2$, which corresponds to $16\ \text{aJ } \mu\text{m}^{-2}$. The total address energy is $E_{\text{Tot}}^A = I\tau$, which gives $E_{\text{Tot}}^A = 5\ \text{fJ}$. Correspondingly, the control density is of about $5\ \text{pol per } \mu\text{m}^2$, which yields $1\ \text{aJ per } \mu\text{m}^2$ ($E_{\text{Tot}}^C = I\tau = 314\ \text{aJ}$). In the calculation, we have used $\tau = 10\ \text{ps}$ as the polariton lifetime (extracted from the polariton linewidth), while $E = 2.39 \times 10^{-19}\ \text{J}$ is the polariton energy and A is the spot area (radius of $10\ \mu\text{m}$). An upper limit can be alternatively obtained from the exciting powers: considering the measured reflection of the address beam from the sample surface (50%), the power of the address is $1.85\ \text{mW}$, and we obtain a density $N = I\tau/(EA) \approx 260\ \text{pol per } \mu\text{m}^2$, which corresponds to $60\ \text{aJ } \mu\text{m}^{-2}$. The total address energy is thus $E_{\text{Tot}}^A = 18.5\ \text{fJ}$. Correspondingly, the control density is of about $20\ \text{pol per } \mu\text{m}^2$, which yields $4\ \text{aJ } \mu\text{m}^{-2}$ ($E_{\text{Tot}}^C = 1.3\ \text{fJ}$).

References

- Paul, B. C., Agarwal, A. & Roy, K. Low-power design techniques for scaled technologies. *Integr. VLSI J* **39**, 64–89 (2006).
- Bohr, M. T. Nanotechnology goals and challenges for electronic applications. *IEEE Trans. Nanotechnol.* **1**, 56–62 (2002).
- Wada, O. Femtosecond all-optical devices for ultrafast communication and signal processing. *New J. Phys.* **6**, 183 (2004).
- Glesk, I. *et al.* All-optical switching using nonlinear subwavelength Mach-Zehnder on silicon. *Opt. Express* **19**, 14031–14039 (2011).
- Johnston, W. J., Prineas, J. P. & Smirl, A. L. Ultrafast all-optical polarization switching in Bragg-spaced quantum wells at 80 K. *J. Appl. Phys.* **101**, 046101 (2007).
- Almeida, V. R., Barrios, C. A., Panepucci, R. R. & Lipson, M. All-optical control of light on a silicon chip. *Nature* **431**, 1081–1084 (2004).
- Nozaki, T. *et al.* Sub-femtojoule all-optical switching using a photonic-crystal nanocavity. *Nat. Photon.* **4**, 477–483 (2010).
- Mori, T., Yamayoshi, Y. & Kawaguchi, H. Low-switching-energy and high-repetition-frequency all-optical flip-flop operations of a polarization bistable vertical-cavity surface-emitting laser. *Appl. Phys. Lett.* **88**, 101102 (2006).

9. Hwang, J. *et al.* A single-molecule optical transistor. *Nature* **460**, 76–80 (2009).
10. Miller, D. A. B. Are optical transistors the logical next step? *Nat. Photon.* **4**, 3–5 (2010).
11. De Giorgi, M. *et al.* Control and ultrafast dynamics of a two-fluid polariton switch. *Phys. Rev. Lett.* **109**, 266407 (2012).
12. Savasta, S., Di Stefano, O. & Giralanda, R. Many-body and correlation effects on parametric polariton amplification in semiconductor microcavities. *Phys. Rev. Lett.* **90**, 096403 (2003).
13. Savvidis, P. G. *et al.* Angle-resonant stimulated polariton amplifier. *Phys. Rev. Lett.* **84**, 1547–1550 (2000).
14. Huang, R., Tassone, F. & Yamamoto, Y. Experimental evidence of stimulated scattering of excitons into microcavity polaritons. *Phys. Rev. B* **61**, R7854–R7857 (2000).
15. Ciuti, C., Schwendimann, P., Deveaud, B. & Quattropani, A. Theory of the angle-resonant polariton amplifier. *Phys. Rev. B* **62**, R4825–R4828 (2000).
16. Stevenson, R. M. *et al.* Continuous wave observation of massive polariton redistribution by stimulated scattering in semiconductor microcavities. *Phys. Rev. Lett.* **85**, 3680–3683 (2000).
17. Saba, M. *et al.* High-temperature ultrafast polariton parametric amplification in semiconductor microcavities. *Nature* **414**, 731–735 (2001).
18. Baas, A., Karr, J. P., Eleuch, H. & Giacobino, E. Optical bistability in semiconductor microcavities. *Phys. Rev. A* **69**, 023809 (2004).
19. Tredicucci, A. *et al.* Optical bistability of semiconductor microcavities in the strong-coupling regime. *Phys. Rev. A* **54**, 3493–3498 (1996).
20. Gippius, N. A., Tikhodeev, S. G., Kulakovskii, V. D., Krizhanovskii, D. N. & Tartakovskii, A. I. Nonlinear dynamics of polariton scattering in semiconductor microcavity: bistability vs. stimulated scattering. *Europhys. Lett.* **67**, 997–1003 (2004).
21. Whittaker, D. M. Numerical modelling of the microcavity OPO. *Phys. Stat. Sol. C* **2**, 733–737 (2005).
22. Gippius, N. A. *et al.* Polarization multistability of cavity polaritons. *Phys. Rev. Lett.* **98**, 236401 (2007).
23. Bajoni, D. *et al.* Optical bistability in a GaAs-based polariton diode. *Phys. Rev. Lett.* **101**, 266402 (2008).
24. Paraíso, T. K., Wouters, M., Léger, Y., Morier-Genoud, F. & Deveaud-Plédran, B. Multistability of a coherent spin ensemble in a semiconductor microcavity. *Nat. Mater.* **9**, 655–660 (2010).
25. Amo, A. *et al.* Exciton-polariton spin switches. *Nat. Photon.* **4**, 361–366 (2010).
26. Kasprzak, J. *et al.* Bose-Einstein condensation of exciton polaritons. *Nature* **443**, 409–414 (2006).
27. Balili, R., Hartwell, V., Snoke, D., Pfeiffer, L. & West, K. Bose-Einstein condensation of microcavity polaritons in a trap. *Science* **316**, 1007–1010 (2007).
28. Amo, A. *et al.* Collective fluid dynamics of a polariton condensate in a semiconductor microcavity. *Nature* **457**, 291–295 (2009).
29. Amo, A. *et al.* Superfluidity of polaritons in semiconductor microcavities. *Nat. Phys.* **5**, 805–810 (2009).
30. Sanvitto, D. *et al.* Persistent currents and quantized vortices in a polariton superfluid. *Nat. Phys.* **6**, 527–533 (2010).
31. Amo, A. *et al.* Polariton superfluids reveal quantum hydrodynamic solitons. *Science* **332**, 1167–1170 (2011).
32. Sanvitto, D. *et al.* All-optical control of the quantum flow of a polariton condensate. *Nat. Photon.* **5**, 610–614 (2011).
33. Christopoulos, S. *et al.* Room-temperature polariton lasing in semiconductor microcavities. *Phys. Rev. Lett.* **98**, 126405 (2007).
34. Liew, T. C. H., Kavokin, A. V. & Shelykh, I. A. Optical circuits based on polariton neurons in semiconductor microcavities. *Phys. Rev. Lett.* **101**, 016402 (2008).
35. Shelykh, I. A., Pavlovic, G., Solnyshkov, D. D. & Malpuech, G. Proposal for a mesoscopic optical berry-phase interferometer. *Phys. Rev. Lett.* **102**, 046407 (2009).
36. Liew, T. C. H. *et al.* Exciton-polariton integrated circuits. *Phys. Rev. B* **82**, 033302 (2010).
37. Wertz, E. *et al.* Spontaneous formation and optical manipulation of extended polariton condensates. *Nat. Phys.* **6**, 860–864 (2010).
38. Johne, R., Shelykh, I. A., Solnyshkov, D. D. & Malpuech, G. Polaritonic analogue of datta and das spin transistor. *Phys. Rev. B* **81**, 125327 (2010).
39. Gibbs, H. M. *Optical Bistability: Controlling Light with Light* (Academic Press, Inc., Orlando, FL, USA, 1985).
40. Cancellieri, E., Marchetti, F. M., Szymańska, M. H., Sanvitto, D. & Tejedor, C. Frictionless flow in a binary polariton superfluid. *Phys. Rev. Lett.* **108**, 065301 (2012).
41. Gao, T. *et al.* Polariton condensate transistor switch. *Phys. Rev. B* **85**, 235102 (2012).

Acknowledgements

We would like to thank A. Bramanti and C. Tejedor for useful discussions, P. Cazzato for the technical assistance with the experiments, and F.M. Marchetti and M.H. Szymanska for the development of the simulation code. We are extremely grateful to F.P. Laussy for his constant support. This work has been funded by the FIRB Italiananonet, the POLATOM ESF Research Networking Program and the ERC project POLAFLOW (grant 308136).

Author contributions

All authors contributed to all aspects of this work.

Additional information

Competing financial interests: The authors declare no competing financial interests.

Reprints and permission information is available online at <http://npg.nature.com/reprintsandpermissions/>

How to cite this article: Ballarini, D. *et al.* All-optical polariton transistor. *Nat. Commun.* **4**:1778 doi: 10.1038/ncomms2734 (2013).

Corrigendum: All-optical polariton transistor

D. Ballarini, M. De Giorgi, E. Cancellieri, R. Houdré, E. Giacobino, R. Cingolani, A. Bramati, G. Gigli & D. Sanvitto

Nature Communications 4:1778 doi: 10.1038/ncomms2734 (2013); Published 30 Apr 2013; Updated 26 Nov 2014

In the key to Fig. 2a of this Article, the units for the control intensity were inadvertently given as mW instead of μW . The correct version of Fig. 2 appears below.

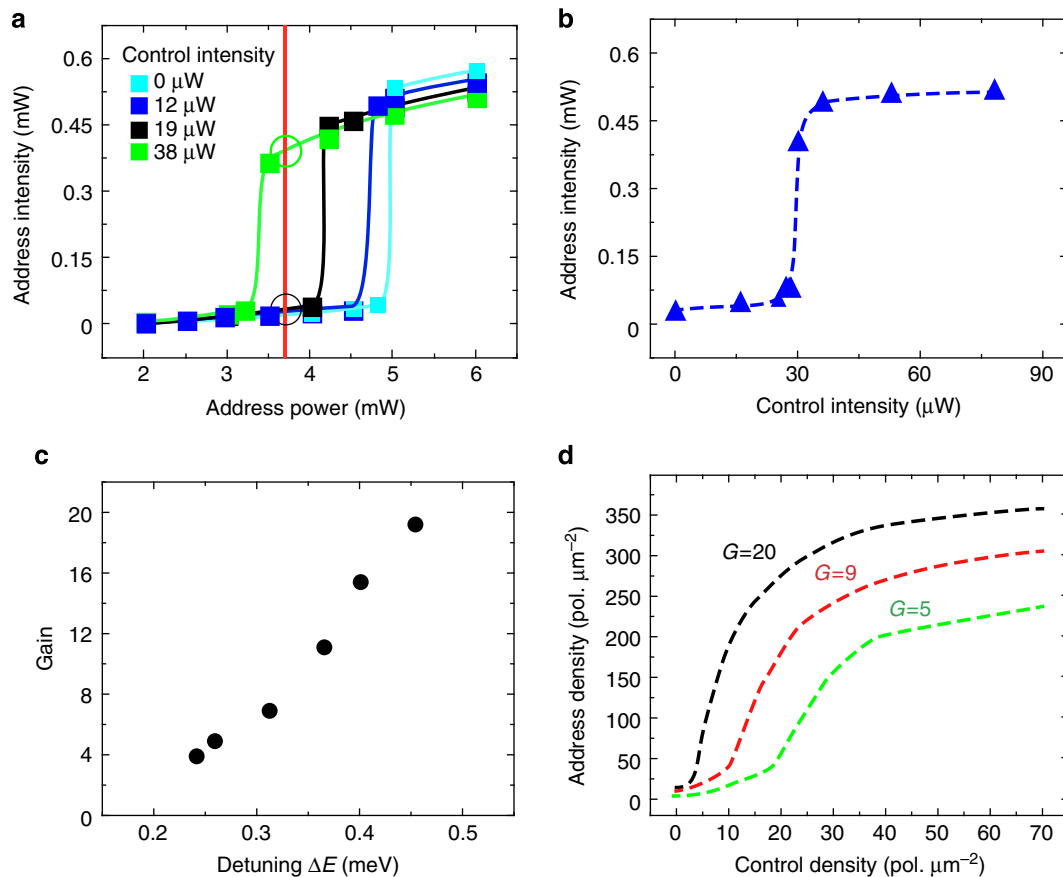


Figure 2